https://doi.org/10.1016/j.apenergy.2020.115004

Comprehensive experimental testing and analysis on parabolic trough solar receiver integrated with radiation shield

Qiliang Wang [a, b], Honglun Yang [b], Shuai Zhong [b], Yihang Huang [b], Mingke Hu [c], Jingyu Cao [b, d], Gang Pei [b, *], Hongxing Yang [a]

[a] *Renewable Energy Research Group (RERG), Department of Building Services Engineering, The Hong Kong Polytechnic University, Hong Kong, China*

[b] *Department of Thermal Science and Energy Engineering, University of Science and Technology of China, Hefei 230027, China*

[c] *Institute of Sustainable Energy Technology, University of Nottingham, University Park, Nottingham NG7 2RD, UK*

[d] *Ability R & D Energy Research Centre, School of Energy and Environment, City University of Hong Kong, Hong Kong, China*

* Corresponding author. E-mail address: peigang@ustc.edu.cn

The short version of the paper was presented at ICAE2019, Aug 12-15, Västerås, Sweden. This paper is a substantial extension of the short version of the conference paper.

Abstract

Parabolic trough collectors (PTCs) are the most mature way to harvest high-temperature heat source and widely applied in solar thermal utilizations. Parabolic trough solar receivers as the heat-collecting elements (HCEs) are the key parts of PTC, but face with a knotty problem that is exploding radiative heat loss under high operating temperature, which exerts a significantly negative role on the overall performance of the PTC system. For effectively reducing the heat loss and improving the

thermal performance of solar receiver, a structurally optimized HCE with an inner radiation shield was proposed, designed, and manufactured. Furthermore, the indoor heat loss and outdoor thermal efficiency testing were carried out in the Institute of Electrical Engineering, Chinese Academy of Sciences (IEECAS) to validate comprehensive thermal performance of the proposed HCEs. The results show that the radiation shield plays an effective role in reducing the heat loss and improving the thermal efficiency. The heat loss of the proposed HCE is significantly reduced by 28.0 % compared to the conventional HCE at the absorber temperature of 550 °C. And the proposed HCE possesses superior performance at high operating temperature and low solar irradiance. In the case of inlet temperature of 350 °C and solar irradiance of 600 W/m^2, the thermal efficiencies of proposed HCE and conventional HCE are 49.4 and 51.8 % respectively, and the thermal efficiency of the proposed HCE is effectively enhanced by 4.9 %.

KEYWORDS: *Parabolic trough collector; PTC; Heat loss; Efficiency; Optimization*

Nomenclature

a	Ambient	in	Inlet
c	Specific heat capacity, J/(kg·K)	**Greek Symbols**	
k	Radiation shield	η	Efficiency
s	Absorber tube	ξ	Incidence angle, °
A	Area, m^2	**Abbreviation and subscripts**	
D	Diameter, mm	HCE	Heat-collecting element
E	Emissive power, W/m2	CHCE	Conventional heat-collecting element
F	Factor view/ Heat removal factor	NHCE	Novel heat-collecting element

L	Length, m	CSP	Concentrated solar power
P	Percentage, %	PTC	Parabolic trough collector
Q	Net heat flux, W/m	HTF	Heat transfer fluid
T	Temperature, K	DNI	Direct normal irradiance, W/m^2
U	Heat loss coefficient, W/(K·m^2)	SSC	Solar selective-absorbing coating
W	Width, m	RS	Radiation shield
ap	Aperture	HL	Heat loss

1. Introduction

At present, parabolic trough collectors (PTCs) are the most mature and commercial technology to achieve high-temperature heat source for solar thermal utilizations [1, 2]. The PTC system includes the trough mirrors, heat-collection elements (HCEs), tracking devices, heat transfer fluid (HTF) flowing in the solar receivers, and so on. HCEs are placed along the focus of the trough mirrors where the direct normal irradiance (DNI) is reflected by the mirrors and concentrated to the HCEs. HCEs are mainly composed of glass envelope, absorber tube, metal bellows [3, 4]. The solar selective-absorbing coating (SSC) is deposited on the outer surface of the absorber tube for ensuring absorber tube high absorptance to the solar irradiance [5]. Then the solar energy captured by the absorber tube is converted into the heat energy of the HTF. After the heat collection in mirror field, the outlet temperature of the HTF can reach different temperature levels for various applications of medium and high-temperature levels, such as solar desalination, solar cooling, processes [6-8], and particularly, concentrated solar power (CSP) [9, 10].

As the key part of the PTC system, HCEs usually operate with thermal oils of Therminol VP-1

for operation up to 400 °C [11, 12]. Besides, HCEs can operate with water/steam for direct-expansion electricity production in Rankine cycles. Moreover, HTF of molten salts is applied into the HCEs and PTC system, which can operate up to 550~600°C [13, 14]. Beside of corrosion under harsh environmental conditions, the deformation and stress rupture under such high temperature need to be overcame for the HCEs. Some researchers brought insight into the nonuniform-temperature-induced deformation of receiver tubes focusing on the thermo-elastics [15, 16], and superheating phenomenon with the highest thermal load [15, 17, 18]. Apart from firm structures and reliable resistant materials, the design core of the HCEs is to maximize the heat gain. The heat gain of the HCEs depends on the absorption of the solar irradiance and the heat loss, thus strengthening the absorption and reducing the heat loss are two main approaches focused by the researchers for enhancing the thermal performance of the HCEs. For effectively blocking heat conduction and convection from the absorber tube, the annular space between the absorber tube and glass envelope is evacuated. The glass envelope uses ultra-white glass due to its high transmittance to the solar irradiance compared with other glasses [19, 20]. In addition, the upper and lower surfaces of glass envelope are deposited with anti-reflective coatings, which contribute to higher transmittance of the solar irradiance and enhance the glass envelope transmittance to 96%. The absorber tube is coated with SSC which has high absorptance of the solar irradiance and low emittance of the infrared radiation [21, 22]. The latest SSC used in the HCEs can reach absorptance of 96% and the emittance of 10% at the absorber temperature of 400 °C. Up to now, the performance enhancement of the SSC is still a research hotspot [23-25].

However, the improvement room of the SSC performance is limited, especially the emittance of the SSC. When the absorber temperature increases, the SSC emittance grows rapidly. In addition, the

blackbody emissive power from the absorber tube increases exponentially to fourth power of the absorber temperature [26]. Thus, the total radiation heat from the absorber tube, which is the product of the emittance and the blackbody emissive power, increases rapidly. To some extent, this phenomenon of high radiation heat loss at high operating temperature in HCEs cannot be solved completely, because the rising SSC temperature inevitably incurs the higher emittance and the blackbody emissive power [27]. Different from the traditional optimization method of enhancing optical performance of the SSC, a novel structural optimization strategy was proposed based on the characteristics of the circumferentially uneven solar irradiance distribution in HCEs [28]. As shown in Fig. 1, the bottom half part of the HCE towards the mirrors receives high-energy density solar irradiance by the mirror concentrator (called ***Concentration part***), but the top half part of the HCE not directly facing the mirrors only receives low-energy density solar irradiance without the projection of the concentrated solar rays (called ***Nonconcentration part***). In the case of sufficiently high operating temperature in HCEs, it is noteworthy that the radiation heat from the absorber tube would exceed the absorbed solar irradiance by the absorber tube in the nonconcentrated part, this rarely discovered phenomenon demonstrates the negative net heat gain occurs in nonconcentration part, and reveals the structural imperfection appearing in the HCEs. For reducing the heat loss in nonconcentration part and thus improving the comprehensive performance in HCEs, we put forward a novel structure of radiation shield (RS), which was placed into the vacuum annular in the nonconcentration part. The proposed RS could intercept much radiation heat from the absorber tube without incurring excessive solar irradiation blockage loss because of received low-energy density solar irradiance in this part. Comprehensively, the net heat gain of the absorber tube in the nonconcentration part could be positively improved after

the structural optimization of adding RS.

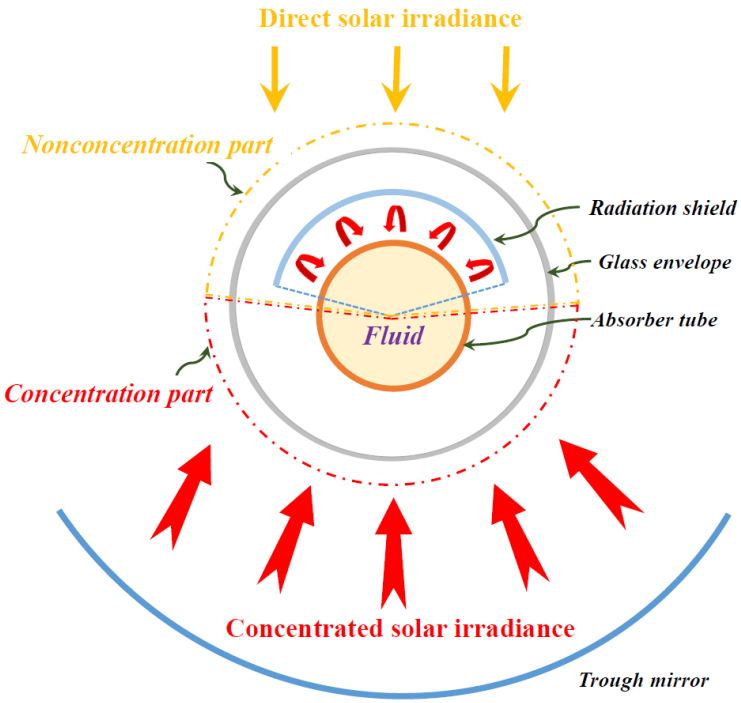

Fig. 1 The schematic diagram of novel HCE with an inner radiation shield

In previous works, we preliminarily conducted indoor heat loss experiments on the unnormalized HCEs with a length of 1.98 m, external diameters of absorber tube and glass envelope of 51 mm and 102 mm respectively [28]. To some extent, however, this work hardly predicts the thermal performance for standard and commercial HCEs due to much different specifications and materials compared with unnormalized one. For the comprehensive investigations and analyses on the overall performance of the standard HCEs used in commercial CSP plants, therefore, we cooperated with the TRX Solar technology Co. Ltd [29] and manufactured the novel HCEs with the RS (NHCEs) based on the conventional standard HCEs (CHCEs). It is worth noting that some design parameters of RS in this study including coating material properties are optimized and different from these of RS in previous work, the detail information is presented in section 2.1. Additionally, we carried out the indoor heat loss and outdoor thermal efficiency testing in the Institute of Electrical Engineering, Chinese Academy

of Sciences (IEECAS), the outdoor testing was accurately realized by the two-axis tracking PTC rotating platform. Furthermore, the influences of the different parameters, namely, absorber temperature, solar irradiance, and inlet temperature, on the overall performance of the NHCEs were also studied.

2. Experimental setups and methodology

2.1 Heat-collection elements

Commercially normal HCE and proposed NHCE were trail-produced as shown in Fig. 2. The basic specifications of the CHCE and NHCE are presented in Table 1, it is noticeable that the radiation shield (RS) employs the aluminum sheet which has light weight and required strength to ensure its stability in the HCE. The view factor F_{sk} is the fraction of energy exiting an absorber tube, that directly impinges on RS. According to the previous study [28], closer distance between the RS and the absorber tube means larger value of F_{sk} and better effect of heat interception by RS. Thus, lesser RS diameter is high priority target, the RS diameter was designed as 80 mm with overall consideration of difficulty of its actual construction. In addition, the angle of RS surrounding the absorber tube was set as 120° for avoiding the interception of the incoming concentrating solar rays by the RS from the trough mirrors. Different from the SSC deposited on the outer surface of RS in previous study, the SSC used in this study employed the ceramic absorbing coating which has lower emittance at high temperature (0.09@400°C), that contributes to reduce more heat loss radiated from the NHCE.

Table 1 Specifications of the tested HCE

Component	Material	Dimension
Glass envelope	Borosilicate glass	Outer diameter: 125 mm Thickness: 2.5 mm
Absorber tube	Stainless steel	Length: 4060 mm Outer diameter: 70 mm Thickness: 3 mm
Radiation shield (NHCE)	Aluminum sheet	Diameter: 80 mm Angle: 120°

As shown in Fig. 2(b), the RS in NHCE was fixed by the thinner metal support frames. A good structural and performance stability of the RS in the NHCE was proved in the whole experiments.

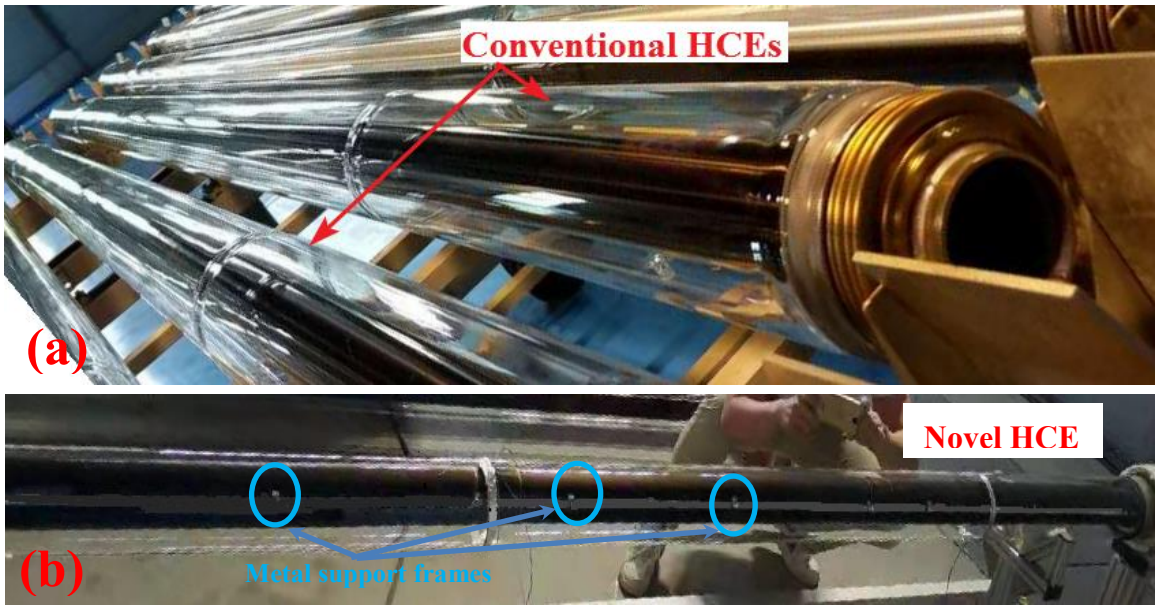

Fig. 2 Trial-manufactured (a) conventional HCE, and (b) novel HCE with an inner radiation shield

2.2 Indoor experiment setup and methodology

The NHCE was tested in the indoor heat loss platform, the detail experimental setups of NHCE were exhibited in Fig. 3. The heat loss experiments were conducted based on the heat equilibrium method using 6 electric heaters [23, 27]. All of six heaters were inserted into a copper tube, the copper

tube was put inside of the absorber tube for circumferential and axial heating uniformity along the absorber tube. Two cartridge heaters were placed along the shaft axis of the copper tube and fixed by structural supports, two innermost coiled cable heaters located at the edges of the absorber tube for the heat compensation to much larger edges' heat loss, and two outermost coiled cable heaters used to create an adiabatic boundary were fixed at the edges of the copper tube.

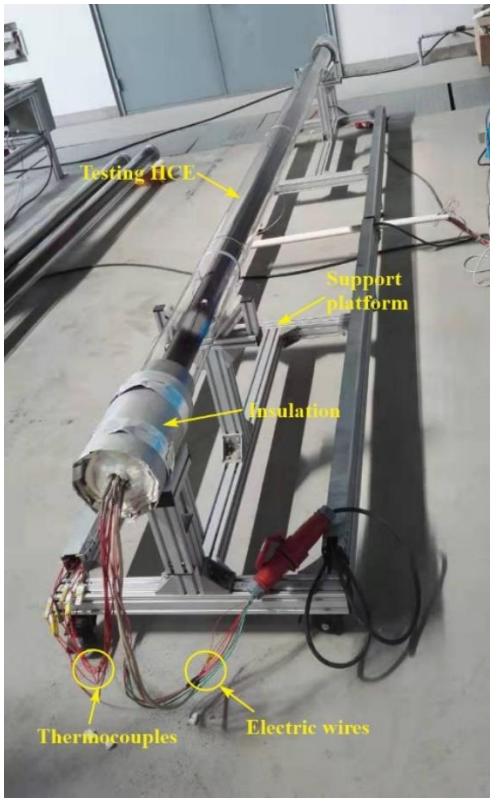

Fig. 3 Indoor testing platform

For accurately monitoring the thermal equilibrium state, total 18 thermocouples were installed. Each effective indoor experimental data was obtained when the monitored absorber temperatures kept within a difference of 10 K and maintained the quasistatic process for 20 mins. The absorber temperature and glass envelope temperature under quasistatic state can be determined by averaging the temperatures monitored by their thermocouples respectively. Furthermore, the direct acquisition of the heaters' powers from the central console enabled the acquisition of the total heat loss from the

tested HCEs, which is the accumulation of two cartridge heaters' and two innermost coiled cable heaters' powers [23]. The total heat loss in the HCE can be expressed as:

$$HL_{HCE} = \frac{Cart1 + Cart2 + Coil1 + Coil2}{L_{HCE}}, \quad (1)$$

where, HL represents the total heat loss, W/m. Cart and Coil are the electric powers of the cartridge heater and innermost coiled cable heater, W. L is the length of HCE, m.

Compared with CHCE, the relative percentage of the heat loss reduction of NHCE-RS in % is expressed as:

$$P_{HL} = \frac{HL_{CHCE} - HL_{NHCE-RS}}{HL_{CHCE}} \times 100\%. \quad (2)$$

2.3 Outdoor experiment setup and methodology

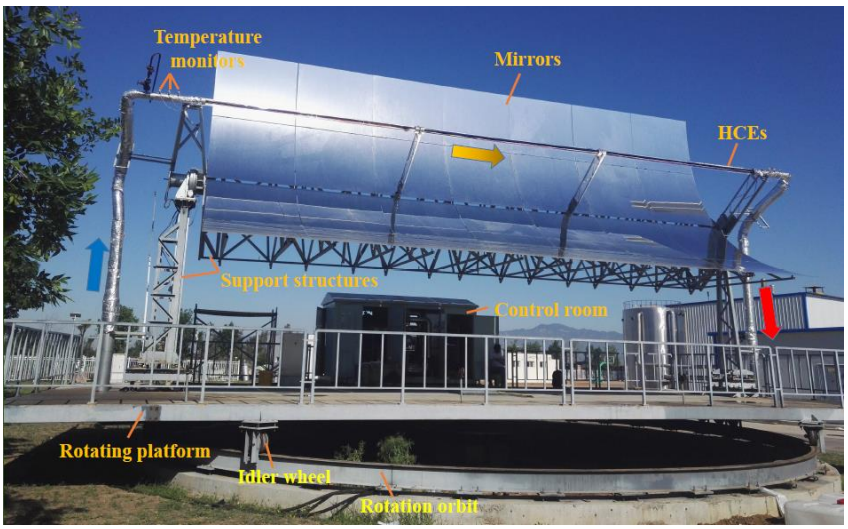

Fig. 4 Outdoor testing platform

To validate the comprehensive performance of the NHCE-RS, we tested the thermal efficiency of the PTC installed with the NHCE-RS on the outdoor parabolic trough collector testing platform in the IEECAS. The specifications of PTC testing platform and measuring devices are presented in Table 2 and Table 3. HTF in PTC system was selected as silicon oil for its high thermodynamic performance

parameter [30]. It is worth noting that the PTC platform tracks the sun with double axes. Besides of the up-and-down tracking, this platform realizes the left-right tracking with high precision by the rotating orbit as shown in Fig. 4. Two-axes tracking contributes much to rigorous and accurate test on the comprehensive performance of NHCE-RS.

Table 2 Specifications of parabolic trough collector testing platform

parameter	Dimension	parameter	Dimension
Length	12 m	Aperture area	69.24 m^2
Width	5.78 m	Concentration ratio	82.6

Table 3 List of outdoor experimental testing and monitoring devices

Device	Specification	Quantity	Accuracy
Pyranometer	SOLYS 2 (KIPPZONEN, Netherlands)	1	±0.5 %
Anemometer	WS601 (Lufft, Germany)	1	±0.3 m/s
Ambient thermometer	WS601 (Lufft, Germany)	1	±0.2 °C
Thermocouple	Pt100 resistance thermometer	4	±0.10 °C
Flowmeter	Vortex flow meter	1	±0.05 m/s
Data logger and computing unit	34980A (Agilent, USA)	1	±0.004 %

The steady-state test method is adopted for the outdoor thermal efficiency test platform. Generally, the experiments were conducted from 10:00 to 14:00 in a day, because the solar irradiance in this time period fluctuates slightly, that is beneficial to realize relative steady-state test. We determined a fixed HTF volume flow rate of 15.0 m^3/h in all experiments. In an experimental process, we set a desired inlet HTF temperature, the auxiliary heating equipment in the testing system will heat the HTF to the set inlet temperature. Once the fluctuation ranges of the inlet temperature and outlet temperature of the PTC testing platform maintain within 0.2 K for 5 mins, the measured data is considered to be valid.

The different inlet HTF temperatures ranging from 200 to 360 °C with an increase interval of about 20 ~ 40 °C were measured. The outdoor experiments were conducted during April to June in 2018.

The thermal efficiency of the PTC in steady-state test can be defined as the heat gain by the HTF in the PTC testing loop divided by the incident solar irradiance on the PTC plane, which is expressed as [31]:

$$\eta = \frac{\dot{m} c_p (T_{\text{out}} - T_{\text{in}})}{DNI \bullet A_{ap} \cos\xi}, \tag{3}$$

where $\dot{m}$ is HTF mass flow rate (kg/s), c_p is HTF specific heat capacity (J/(kg·K)), T_{in} and T_{out} are the inlet and outlet HTF temperatures (K), *DNI* represents the direct normal irradiance (W/m^2). A_{ap} is aperture area of the PTC (m^2). ξ is the angle between the normal line of the aperture plane and the incoming solar ray (rad). The value of ξ is 0 in this study because of two-dimensional tracking employed in the PTC testing platform, thus cosine constant factor value is 1.

Compared with the CHCE, the relative percentage of thermal efficiency increase of the NHCE-RS in % can be expressed as:

$$P_\eta = \frac{\eta_{NHCE-RS} - \eta_{CHCE}}{\eta_{CHCE}} \times 100\%, \tag{4}$$

where, η is the measured thermal efficiency of the PTC.

To eliminate the effect of solar irradiance variation during the quasistatic test process and temperature difference between the surroundings and HTF at the collector inlet, the Hottel-Whillier model was usually applied to obtain general conclusions. The heat gain of the PTC can be expressed as [32]:

$$Q_{gain} = A_{ap}[DNI \bullet F_R(\tau\alpha)_e - F_R U_L (T_{f,av} - T_a)], \tag{5}$$

where F_R is the heat removal factor of the PTC, $(\tau\alpha)_e$ represents the effective product of the glass envelope transmittance and absorber tube absorptance, U_L is the heat loss coefficient of the HCE (W/(K·m^2)), $T_{f,av}$ is the average fluid temperature (K), and T_a is ambient temperature (K). Thus, the thermal efficiency of the PTC can be plotted as a function of temperature difference divided by *DNI*, expressed as [32]:

$$\eta = F_R(\tau\alpha)_e - F_R U_L \frac{T_{f,av} - T_a}{DNI}, \tag{6}$$

where $\frac{T_{f,av} - T_a}{DNI}$ is reduced temperature, (K·m^2)/W; the intercept $F_R(\tau\alpha)_e$ represents the thermal efficiency of the PTC at zero-reduced temperature, also indicated as η_0. Slope $F_R U_L$ represents the heat loss of the HCE.

However, the heat loss of the HCE strongly varies with the absorber temperature, the fixed slope coefficient is incapable of fitting well to the experimental data. For accurate description of general characteristic of the thermal performance of the HCE, the thermal efficiency of the PTC can be expressed as the optical efficiency minus an efficiency penalty term (η') [33],

$$\eta = \eta_0 - \eta'. \tag{7}$$

The value of η' can be achieved by the expression as follows:

$$\eta' = \frac{nHL}{A_{ap} DNI \cos\xi}, \tag{8}$$

where, n is the number of the HCEs contained in the PTC testing platform. As aforementioned, the HCE heat loss is virtually proportional to the absorber temperature raised to the third or fourth power, thus η' would be dependent of the HTF temperature raised to second (or third) power. Thus typical efficiency expression usually includes quadratic item and is written as:

$$\eta^{'} = A\frac{T_{f,av}-T_a}{DNI} + B\frac{(T_{f,av}-T_a)^2}{DNI}. \quad (9)$$

where A and B are coefficients responding to the linear item and quadratic item. According to the research result of Kutscher et al. [33], the efficiency curves plotted versus $(T_{f,av}-T_a)$ under various solar irradiance could appear deviation and cannot be collapsed onto one single curve. But this problem would be solved by changing the exponent of *DNI*, it means the various radiation curves can be collapsed into a single curve by dividing the temperature difference by *DNI* raised to a fractional power, which eliminates the uncertainty associated with trying to interpolate between different radiation curves. Hence, the abscissa of the temperature difference divided by the *DNI* raised to a fractional power was employed to collapse various radiation curves into a single curve. For keeping same exponent of -1 of *DNI* at the quadratic item in Equation (9), the exponent of *DNI* in this paper is determined as 0.5, thus the expression of the thermal efficiency plotted versus reduced temperature $(\frac{T_{f,av}-T_a}{DNI^{0.5}})$ can be written as [33]:

$$\eta = \eta_0 - A\frac{T_{f,av}-T_a}{DNI^{0.5}} - B(\frac{T_{f,av}-T_a}{DNI^{0.5}})^2, \quad (10)$$

2.4 Error analysis

The relative error (RE) of the heat loss and thermal efficiency can be described as follows [33, 34]:

$$RE_{HL} = \frac{dHL}{HL} = d(\frac{Cart1+Cart2+Coil1+Coil2}{L_{HCE}}) / \frac{Cart1+Cart2+Coil1+Coil2}{L_{HCE}} \quad (11)$$

$$RE_{\eta} = \frac{d\eta}{\eta} = d(\frac{\dot{m}c_p(T_{\text{out}}-T_{\text{in}})}{DNI \bullet A_{ap}}) / \frac{\dot{m}c_p(T_{\text{out}}-T_{\text{in}})}{DNI \bullet A_{ap}} \quad (12)$$

According to the calculation results based on the Equation (11) ~ (12), the values of RE_{HL} and

RE_η of the heat loss and thermal efficiency remain within 4.5 % and 7.0 %, respectively, which demonstrate the experimental data has a good reliability to be used for analyses.

3. Results and discussions

3.1 Quasi-steady state process

The indoor heat loss and outdoor thermal efficiency experiments were conducted in September to October 2017, and April to June 2018. The absorber temperatures *Abs1~Abs4* monitored by thermocouples and the powers of electric heaters including cartridge heaters and coiled cable heaters under the quasi-steady state were monitored as shown in Fig. 5, this experiment was performed during 11:33:33~12:00:13 at 27 Sep. 2017, it achieved duration time of 27 mins under the quasi-steady state and met valid measurement requirement. Fig. 6 shows the approaching process of the HTF temperature elevating to a relatively steady temperature. This experiment was conducted in 22 May 2018, the quasi-steady state maintained 6 mins from approximate 12:57:00 to 13:03:00, during which the mean solar irradiance was about 705 W/m^2 and its fluctuation was within ±10 W/m^2.

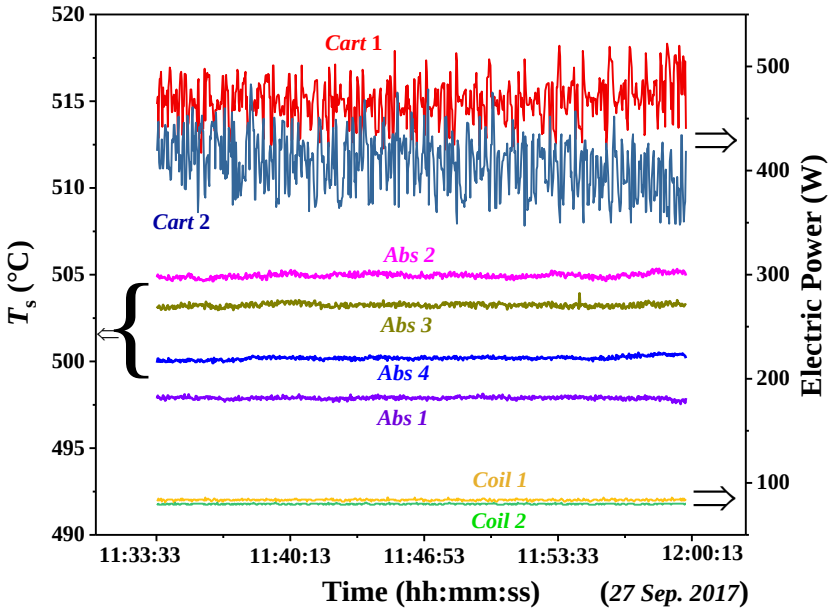

Fig. 5 Indoor heat loss experimental process under quasi-steady state

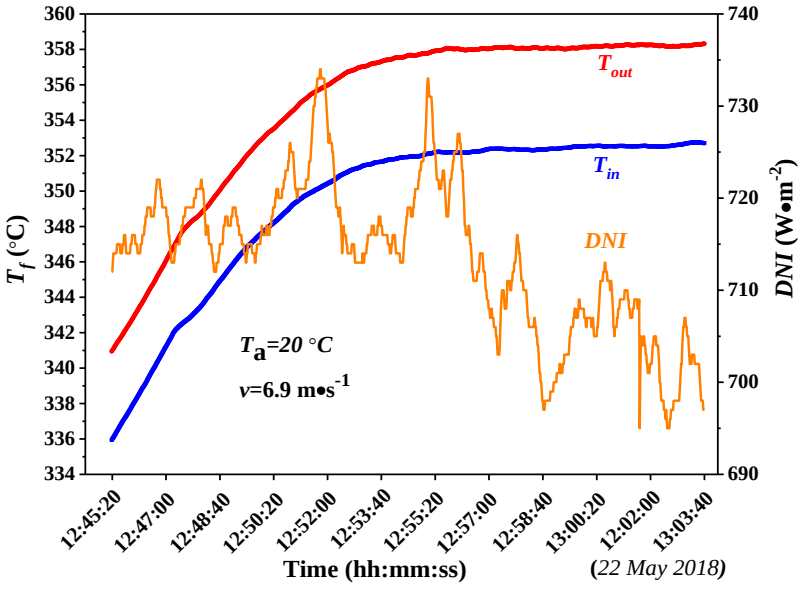

Fig. 6 Outdoor thermal efficiency experimental process approaching gradually to quasi-steady state. This experimental process was measured under ambient temperature (T_a) of 20 °C and wind speed (v) of 6.9 m/s.

3.2 Indoor heat loss

The heat losses of CHCE and NCHE-RS in response to different absorber temperature ranging from approximate 200 to 550 °C are presented in Fig. 7. The indoor ambient temperature in the experiments was around 23 °C. We employ polynomial fit to greatly draw all experimental data near the fitting curve.

As shown in Fig. 7, the NHCE-RS possesses obviously superior heat loss performance compared to the CHCE. The heat loss of the NCHE-RS has been below that of the CHCE from the 200 to 550 °C, and the reduced heat loss of the NCHE-RS compared to the CHCE enlarges with the increasing absorber temperature, which can be demonstrated by the percentage of heat loss reduction in Fig. 8. It can be seen that the percentage of heat loss reduction in % of NHCE-RS compared to the CHCE gradually improves with the increasing absorber temperature, which illustrates that the RS plays more

effective role in reducing the heat loss at higher temperature. This phenomenon occurs because the absorber tube with higher temperature emits much larger amount of heat loss, the RS could intercept much more emissive heat from the absorber tube and thereby work more effectively. When the absorber temperature is 550 °C, the heat losses of the CHCE and NHCE-RS are 657.9 W/m^2 and 473.9 W/m^2 respectively, the latter is effectively reduced by 28.0 % compared to the former.

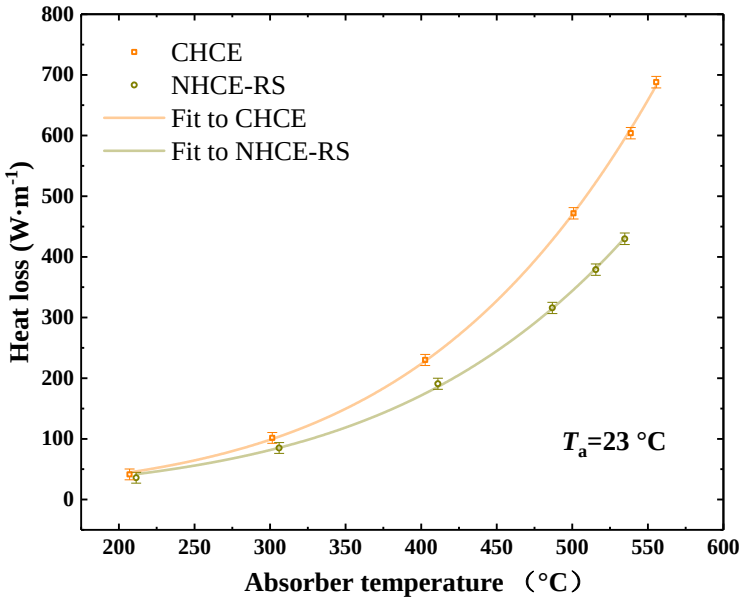

Fig. 7 Experimental heat loss results of CHCE and NHCE-RS

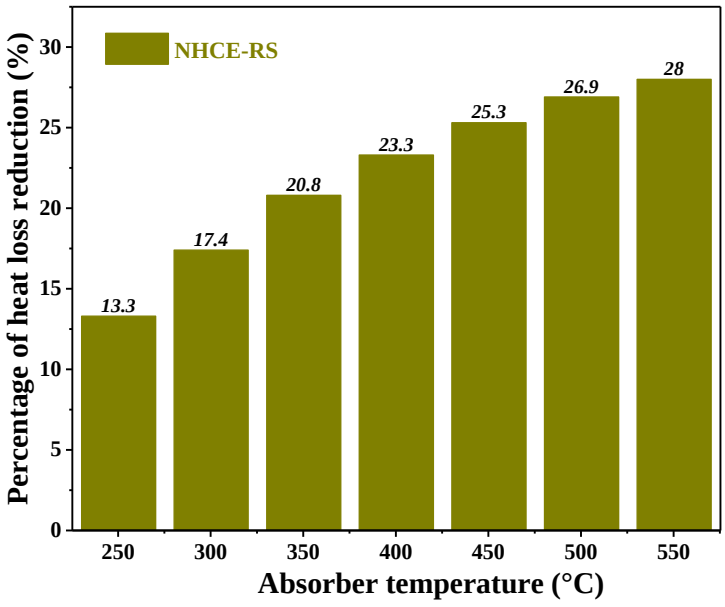

Fig. 8 Percentage of heat loss reduction of the NHCE-RS compared to CHCE

3.3 Outdoor thermal efficiency

The environmental parameters such as *DNI*, ambient temperature and so on exert influences on the thermal efficiency of the PTC. As explained before, to eliminate the influences of the *DNI* and ambient temperature and make curve fit well to the experiment data, we set the abscissa as the temperature difference divided by *DNI* raised to half power. We selected valid experimental data of NHCE-RS and CHCE which meets the requirements of measured *DNI* approximately from 700 W/m^2 to 860 W/m^2 and inlet temperature from 300 °C to 360 °C, and plotted the efficiency curves. As shown in Fig. 9, according to the Equation (9) the expressions of the thermal efficiencies of the PTC with the CHCE and NHCE-RS against $(T_{f,av}-T_a)/DNI^{0.5}$ are fitted as follows:

$$\eta_{CHCE} = 82.52 - 0.01\frac{T_{f,av}-T_a}{DNI^{0.5}} - 0.17(\frac{T_{f,av}-T_a}{DNI^{0.5}})^2, \tag{13}$$

$$\eta_{NHCE-RS} = 79.58 - 0.50\frac{T_{f,av}-T_a}{DNI^{0.5}} - 0.09(\frac{T_{f,av}-T_a}{DNI^{0.5}})^2. \tag{14}$$

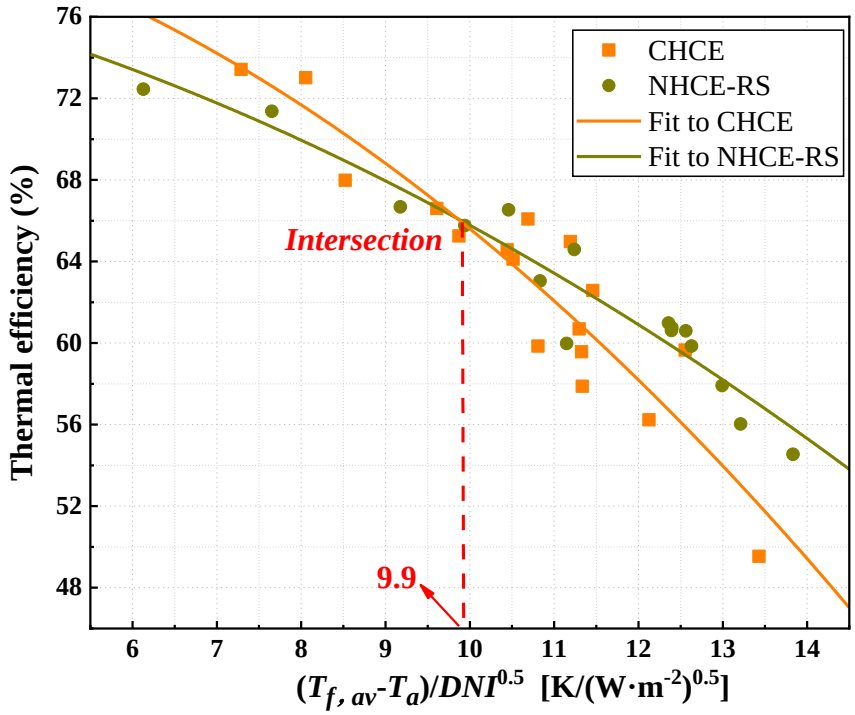

Fig. 9 Plot of thermal efficiencies of PTC with CHCE and NHCE-RS

We learn that the efficiency of the NHCE-RS at zero-reduced temperature is 79.58 %, which is lower than that of 82.52 % in CHCE. That is because the RS in NHCE-RS inevitably blocks the incident solar rays from the sun, thus resulting in lower optical efficiency in NHCE-RS. Just as our estimation, RS introduced into vacuum annular exerts negative role in enhancement of thermal performance of HCE at the lower operating temperature. As seen obviously in Fig. 9, however, a slower descent of thermal efficiency occurs in NHCE-RS compared to CHCE, which reflects that the heat loss coefficient of the NHCE-RS is lower than that of the CHCE, and demonstrates that RS contributes to the heat loss reduction of the NHCE compared with the CHCE. Additionally, the slope of fitting curve of NHCE lowers compared with that of CHCE with the increase of reduced temperature, that demonstrates RS is gradually tending to exert much more positive role in reducing heat loss and thus enhancing thermal performance of NHCE-RS at high reduced temperature.

It is noticed that two curves intersect at the $(T_{f,av}-T_a)/DNI^{0.5}$ of 9.9, which means the NHCE-RS

possesses inferior performance in comparison to the CHCE at the $(T_{f,av}-T_a)/DNI^{0.5}$ value below 9.9, but reverse relationship occurs at the $(T_{f,av}-T_a)/DNI^{0.5}$ value above 9.9. Lower $(T_{f,av}-T_a)/DNI^{0.5}$ value means lower inlet temperature or high solar irradiance at which larger interception loss of solar irradiance by the RS appears compared with the blocked radiation heat loss by the RS in NHCE, and thus lowering the thermal efficiency of NCHE-RS. By contrast, RS intercepts larger heat loss than the incurring solar irradiance in the case of higher inlet temperature or lower solar irradiance, in other words, higher $(T_{f,av}-T_a)/DNI^{0.5}$ value; this leads to higher thermal efficiency in NHCE-RS surpassing CHCE. Assumed that the ambient temperature and solar irradiance are 23 °C and 800 W/m^2, the calculated fluid temperature corresponding to the intersection point in Fig. 9 is about 303.0 °C, which means the NHCE-RS has better thermal performance compared with CHCE at the average fluid temperature exceeding 303.0 °C.

To further verify the performance of NHCE-RS under different *DNI* values and fluid temperatures, the thermal efficiency experiments of NHCE-RS and CHCE under different values of *DNI* in the case of inlet temperature of 300 °C and 350 °C were conducted. The average ambient temperature in the experiments is about 23 °C. The experimental results are exhibited in Fig. 10 and Fig. 11.

In the case of inlet temperature of 300 °C, the NHCE-RS has higher thermal efficiency than CHCE when *DNI* is lower than approximately 800 W/m^2, but the reverse relationship of them appears when *DNI* exceeds 800 W/m^2. As explained above, RS would intercept the incident solar irradiance and thus reduce a certain amount of solar absorption by the absorber tube. However, the amount of solar absorption loss is limited and thus lower than the reduced heat loss by the RS when the *DNI* is lower, which enables NHCE to have higher heat gain and thermal efficiency at lower *DNI*. Then with the increase of *DNI*, the turning point occurs at the *DNI* of about 800 W/m^2. The thermal efficiency of

CHCE gradually approaches that of NHCE-RS and equality between them appears until *DNI* increases to about 800 W/m^2, moreover, the higher thermal efficiency of CHCE is obtained compared with the NCHE-RS at the *DNI* exceeding 800 W/m^2. The reason for this phenomenon is that the amount of solar absorption loss grows with the increasing *DNI*, and finally equals to the reduced radiation heat loss by the RS until *DNI* reaches 800 W/m^2. Correspondingly, the heat gain and thermal efficiency of NHCE-RS and CHCE are also equal at the *DNI* of about 800 W/m^2. And in the case of the *DNI* exceeding 800 W/m^2, the thermal efficiency of CHCE surpasses that of NHCE-RS due to larger amount of solar absorption loss in NHCE-RS.

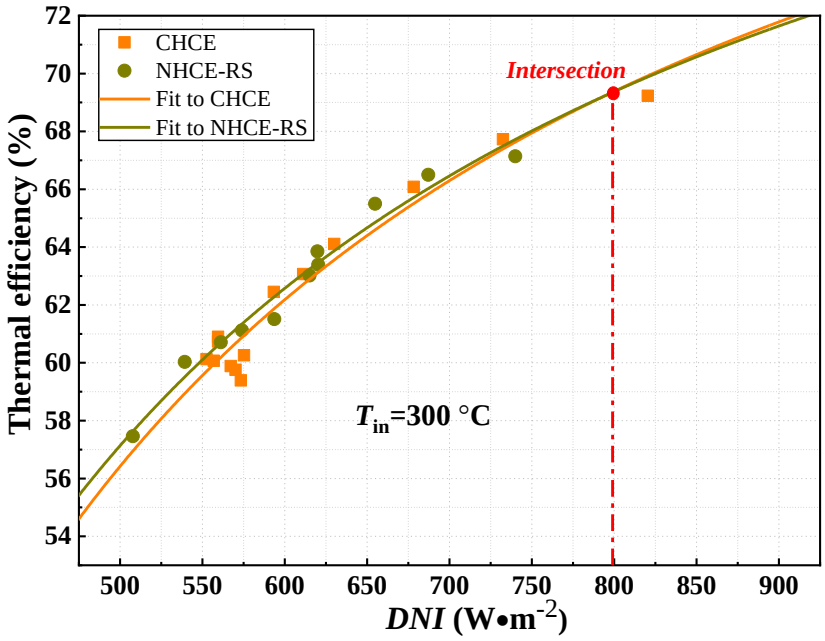

Fig. 10 Thermal efficiencies of CHCE and NHCE-RS against *DNI* at the inlet temperature of 300 °C

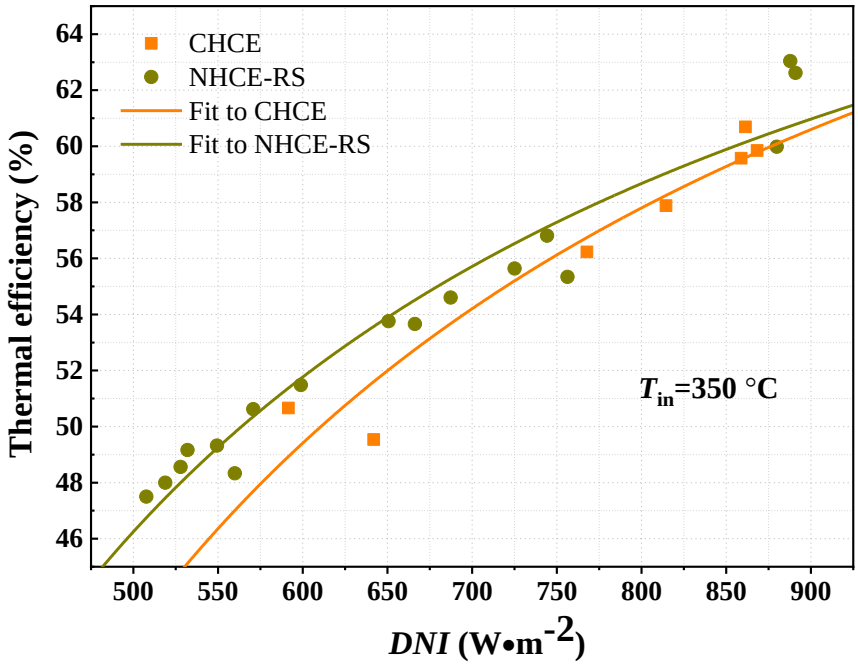

Fig. 11 Thermal efficiencies of CHCE and NHCE-RS against *DNI* at the inlet temperature of 350 °C

In the case of inlet temperature of 350 °C, the NHCE-RS has superior thermal performance than the CHCE at the *DNI* from the 475 to 925 W/m^2 as shown in Fig. 11. Similar to above explanation, this phenomenon is because the absorber tube radiates a large amount of heat loss at high inlet temperature of 350 °C, the reduced heat loss by RS thereby is large enough to surpass the incurred solar absorption loss due to the existence of RS at the *DNI* from the 475 to 925 W/m^2. However, inevitably, the thermal efficiency of CHCE gradually approaches that of NHCE-RS with the increasing *DNI* value because of larger solar absorption loss with response to the increasing solar irradiance.

Table 4 Enhanced thermal efficiency of NHCE-RS at the inlet temperature of 350 °C under different *DNI* values

Type	600 W/m^2		700 W/m^2		800 W/m^2	
	η (%)	P_η (%)	η (%)	P_η (%)	η (%)	P_η (%)
CHCE	49.4	\	54.2	\	57.8	\
NHCE-RS	51.8	4.9	55.7	2.8	58.7	1.6

The thermal efficiencies of CHCE and NHCE-RS at the inlet temperature of 350 °C under different *DNI* values are exhibited in Table 4. These two types of HCEs have higher thermal efficiency

at higher *DNI* value, but the NHCE-RS possesses better performance compared with CHCE. When the *DNI* value is 600 W/m^2, the thermal efficiencies of CHCE and NHCE-RS are 49.4 and 51.8 %, the latter effectively improves by 4.9 % compared with the former.

For observing the realistic performance of NHCE-RS, we selected two typical places with many commercial application cases of PTC system as study examples, i.e., Mojave Desert of California in USA and Dunhuang City in China. Based on above thermal efficiency fittings and analyses, the mean annual efficiency of NHCE-RS and CHCE under inlet temperature of 350 °C the real *DNI* in Mojave Desert and Dunhuang City. The results are presented in Table 5, it can be observed that NHCE-RS exerts more effective role in enhancing the mean annual efficiency at the Dunhuang City which has lower mean annual *DNI* compared with Mojave Desert. The enhancement percentages of mean annual efficiencies in NHCE-RS at Mojave Desert and Dunhuang City are 2.3 % and 5.1 %, respectively, compared with these of CHCE.

Table 5 Mean annual efficiencies in Mojave Desert and Dunhuang City

Region	Location	Climate	Mean Annual *DNI* (W/m^2)	η_{CHCE} (%)	$\eta_{NHCE\text{-}RS}$ (%)	P_η (%)
Mojave Desert	Southwest USA	Desert climate	737.0	55.6	56.9	2.3
Dunhuang City	Northwest China	Warm temperate climate	586.6	48.6	51.1	5.1

4. Conclusions

For effectively reducing the heat loss and improving the overall performance, a novel heat-collecting element with an inner radiation shield (NHCE-RS) in the parabolic trough collector (PTC) system was proposed, designed, trial-manufactured in this paper. The indoor heat loss and outdoor

thermal efficiency of the proposed NCHE-RS were tested to verify its performance. The results are summarized as follows:

(1) The radiation shield (RS) exerts an effective role in reducing heat loss. The heat losses of NHCE-RS and conventional HCE (CHCE) are 473.9 W/m^2 and 657.9 W/m^2 respectively, and the heat loss of the NHCE-RS is relatively reduced by 28.0 % compared to the CHCE.

(2) The NHCE-RS has superior thermal efficiency at the operating temperature above about 303 °C in the case where the ambient temperature and solar irradiance are 23 °C and 800 W/m^2, respectively. Therefore, NHCE-RS can be definitely applied to the commercial PTC system in which the operating temperature reaches 400-550 °C.

(3) NHCE-RS possesses superior thermal efficiency at higher operating temperature or lower solar irradiance. When the *DNI* and inlet temperature are 600 W/m^2 and 350 °C, the thermal efficiencies of CHCE and NHCE-RS are 49.4 and 51.8 %, the NHCE-RS effectively improves thermal efficiency by 4.9 % compared with CHCE. Furthermore, the enhancement percentages of mean annual efficiencies in NHCE-RS at Mojave Desert and Dunhuang City are 2.3 % and 5.1 %.

Acknowledgments

This study was sponsored by National Key R&D Program of China (2018YFB1900602), National Science Foundation of China (51761145109, 51776193), China Postdoctoral Science Foundation (2019M652209), and the ITF Postdoctoral Hub programme of The Hong Kong SAR Government, China.

References

[1] Bellos E, Tzivanidis C. Alternative designs of parabolic trough solar collectors. Progress in Energy

and Combustion Science 2019; 71: 81-117.

[2] Fan M, You S, Xia J, Zheng W, Zhang H, Liang H, et al. An optimized Monte Carlo ray tracing optical simulation model and its applications to line-focus concentrating solar collectors. Applied energy 2018; 225: 769-81.

[3] Behar O, Khellaf A, Mohammedi K. A novel parabolic trough solar collector model–Validation with experimental data and comparison to Engineering Equation Solver (EES). Energy Conversion and Management 2015; 106: 268-81.

[4] Wang Q, Hu M, Yang H, Cao J, Li J, Su Y, et al. Performance evaluation and analyses of novel parabolic trough evacuated collector tubes with spectrum-selective glass envelope. Renewable energy 2019; 138: 793-804.

[5] Yang H, Wang Q, Huang Y, Feng J, Ao X, Hu M, et al. Spectral optimization of solar selective absorbing coating for parabolic trough receiver. Energy 2019; 183: 639-50.

[6] Askari I B, Ameri M. The application of linear Fresnel and parabolic trough solar fields as thermal source to produce electricity and fresh water. Desalination 2017; 415: 90-103.

[7] Zhai H, Dai Y J, Wu J Y, Wang R Z. Energy and exergy analyses on a novel hybrid solar heating, cooling and power generation system for remote areas. Applied Energy 2009; 86(9): 1395-404.

[8] Hong H, Liu Q, Jin H. Operational performance of the development of a 15 kW parabolic trough mid-temperature solar receiver/reactor for hydrogen production. Applied energy 2012; 90(1): 137-41.

[9] Zhang H L, Baeyens J, Degrève J, Cacères G. Concentrated solar power plants: Review and design methodology. Renewable and sustainable energy reviews 2013; 22: 466-81.

[10] Vignarooban K, Xu X, Arvay A, Hsu K, Kannan AM. Heat transfer fluids for concentrating solar power systems–a review. Applied Energy 2015; 146: 383-96.

[11] Mwesigye A, Yılmaz İ H, Meyer J P. Numerical analysis of the thermal and thermodynamic performance of a parabolic trough solar collector using SWCNTs-Therminol® VP-1 nanofluid. Renewable energy 2018; 119: 844-62.

[12] Wang Q, Yang H, Hu M, Huang X, Li J, Pei G. Preliminary performance study of a high-temperature parabolic trough solar evacuated receiver with an inner transparent radiation shield. Solar Energy 2018; 173: 640-50.

[13] Ruegamer T, Kamp H, Kuckelkorn T, Schiel W, Weinrebe G, Nava P, et al. Molten salt for parabolic trough applications: system simulation and scale effects. Energy Procedia 2014; 49: 1523-32.

[14] Bradshaw R W, Cordaro J G, Siegel N P. Molten nitrate salt development for thermal energy storage in parabolic trough solar power systems[C]//ASME 2009 3rd International Conference on Energy Sustainability collocated with the Heat Transfer and InterPACK09 Conferences. American Society of Mechanical Engineers Digital Collection 2010: 615-24.

[15] Fuqiang W, Qingzhi L, Huaizhi H, Jianyu T. Parabolic trough receiver with corrugated tube for improving heat transfer and thermal deformation characteristics. Applied energy 2016; 164: 411-24.

[16] Li L, Sun J, Li Y. Prospective fully-coupled multi-level analytical methodology for concentrated solar power plants: general modelling. Applied Thermal Engineering 2017, 118: 171-87.

[17] Fuqiang W, Jianyu T, Lanxin M, Chengchao W. Effects of glass cover on heat flux distribution for

tube receiver with parabolic trough collector system. Energy Conversion and Management 2015; 90: 47-52.

[18] Serrano-Aguilera J J, Valenzuela L, Parras L. Thermal 3D model for direct solar steam generation under superheated conditions. Applied energy 2014; 132: 370-82.

[19] Wang Q, Hu M, Yang H, Cao J, Li J, Su Y, et al. Energetic and exergetic analyses on structural optimized parabolic trough solar receivers in a concentrated solar–thermal collector system. Energy 2019; 171: 611-23.

[20] Xie W T, Dai Y J, Wang R Z. Numerical and experimental analysis of a point focus solar collector using high concentration imaging PMMA Fresnel lens. Energy Conversion and Management 2011; 52(6): 2417-26.

[21] Solar S. Schott PTR 70 Receiver—Setting the Benchmark. Mainz, Germany, 2011.

[22] Jiang D, Yang W, Tang A. A refractory selective solar absorber for high performance thermochemical steam reforming. Applied energy 2016; 170: 286-92.

[23] Burkholder F, Kutscher C. Heat loss testing of Schott's 2008 PTR70 parabolic trough receiver. National Renewable Energy Lab. (NREL), Golden, CO (United States), 2009.

[24] Ahmadi M H, Ghazvini M, Alhuyi Nazari M, et al. Renewable energy harvesting with the application of nanotechnology: A review. International Journal of Energy Research 2019; 43(4): 1387-410.

[25] Wang X, Yu X, Fu S, Lee E, Kekalo K, Liu J. Design and optimization of nanoparticle-pigmented solar selective absorber coatings for high-temperature concentrating solar thermal systems. Journal of Applied Physics 2018; 123(3): 033104.

[26] Holman J P. Heat transfer, New York: McGraw-Hill Inc, 2002; 420-60.

[27] Wang Y M, Tian H, Shen X E, Wen L, Ouyang J H, et al. An elevated temperature infrared emissivity ceramic coating formed on 2024 aluminium alloy by microarc oxidation. Ceramics International 2013, 39(3): 2869-75.

[28] Wang Q, Li J, Yang H, Su K, Hu M, Pei G. Performance analysis on a high-temperature solar evacuated receiver with an inner radiation shield. Energy 2017; 139: 447-58.

[29] Wang Y, Yang L, Wang X, Chen H, Fan H, Taylor RA. CFD simulation of an intermediate temperature, two-phase loop thermosiphon for use as a linear solar receiver. Applied Energy 2017; 207: 36-44.

[30] Willwerth L, Feldhoff J F, Krüger D, et al. Experience of operating a solar parabolic trough direct steam generation power plant with superheating. Solar Energy 2018; 171: 310-19.

[31] Hu M, Pei G, Wang Q, Li J, Wang Y, Ji J. Field test and preliminary analysis of a combined diurnal solar heating and nocturnal radiative cooling system. Applied energy 2016; 179: 899-908.

[32] Duffie J A, Beckman W A, Blair N. Solar Engineering of Thermal Processes, Photovoltaics and Wind[M]. John Wiley & Sons, 2020.

[33] Kutscher C, Burkholder F, Kathleen Stynes J. Generation of a parabolic trough collector efficiency curve from separate measurements of outdoor optical efficiency and indoor receiver heat loss. Journal of solar energy engineering, 2012, 134(1).

[34] Gang P, Guiqiang L, Xi Z, Jie J, Yuehong S. Experimental study and exergetic analysis of a CPC-type solar water heater system using higher-temperature circulation in winter. Solar Energy 2012; 86(5): 1280-6.